Journal of Natural Gas Science and Engineering 107 (2022) 104798

Contents lists available at ScienceDirect

Journal of Natural Gas Science and Engineering

journal homepage: www.elsevier.com/locate/jngse

Effect of wettability of shale on CO_2 sequestration with enhanced gas recovery in shale reservoir: Implications from molecular dynamics simulation

Kanyuan Shi [a,b], Junqing Chen [a,c,d,*], Xiongqi Pang [a,b,**], Fujie Jiang [a,b], Shasha Hui [a,b], Hong Pang [a,b], Kuiyou Ma [a,b], Qi Cong [d]

[a] State Key Laboratory of Petroleum Resources and Prospecting, China University of Petroleum, Beijing, 102249, China
[b] College of Geosciences, China University of Petroleum, Beijing, 102249, China
[c] Beijing Key Laboratory of Optical Detection Technology for Oil and Gas, China University of Petroleum, Beijing, 102249, China
[d] Basic Research Center for Energy Interdisciplinary, College of Science, China University of Petroleum, Beijing, 102249, China

ARTICLE INFO

Keywords:
Wettability
Contact angle
Shale
Molecular dynamics
CO_2 sequestration with enhanced gas recovery

ABSTRACT

The wettability of rock affects the interaction between CO_2, brine, and shale formation, which affects CO_2 sequestration with enhanced gas recovery (CS–EGR) project. However, under reservoir conditions, there is limited research on the surface wettability of shale organic matter, and its internal interaction mechanism is unclear. In this study, the effects of temperature, pressure, mineralization, and concentration ratio of CO_2 to CH_4 on the contact angle were studied using molecular dynamics (MD), and the results were compared with the previous experimental data. Under a certain pressure, the water wettability increases with the increase in temperature. At a fixed temperature, the contact angle of water on graphene increases with the increase of CO_2 pressure. Above the critical pressure, water at different temperatures is wetted by CO_2 on the surface of graphene, and the wettability reversal occurs. The water wettability decreases with the increase in solution salinity. Under the same concentration of droplets, Mg^{2+} and Ca^{2+} have a greater effect on the wetting angle than Na^{+}. The adsorption capacity of the graphene surface for CO_2 is stronger than that of CH_4. Finally, the order of wettability is verified by interaction energy. This study will contribute to alleviating the greenhouse effect.

1. Introduction

Carbon capture and geological storage (CCGS) technology is a technology that reduces carbon dioxide in the atmosphere by injecting and storing it underground (Belhaj et al., 2013; Fan et al., 2019; Zhou et al., 2020). The development and implementation of CCGS technology have attracted attention because of the excessive emission of carbon dioxide, which is the main cause of global warming (Ajayi et al., 2019; Liu et al., 2021; Muhammad et al., 2021). Experts around the world began to realize CCGS technology from all aspects. In this study, the widely distributed shale gas in the world has attracted in-depth research from experts around the globe (Xu et al., 2022; Ge et al., 2022; Yuan et al., 2015). Shale gas is now a potential substitute for traditional fossil resources because of its rich resources and environmental friendliness (Yuan et al., 2015; Paylor, 2017; Hu et al., 2018; Huang et al., 2019; Feng et al., 2022; Tang et al., 2022). In addition, when CO_2 is injected into shale gas reservoir, CO_2 molecules are adsorbed on pore surfaces to replace adsorbed CH_4, which reduces the CO_2 emission in the atmosphere and improves natural gas recovery (Tayari et al., 2015; Birkholzer et al., 2015; Famoori et al., 2021). Therefore, CS-EGR is proposed as an effective means to achieve CCGS and has received attention globally (Louk et al., 2017; Singh et al., 2018; Xu et al., 2020; Muhammad et al., 2022).

The wettability of the reservoir affects the distribution and flow trend of fluid in rock pores, as well as the interaction between CO_2, brine, and shale formation, which contributes to the CS–EGR project implementation (Morrow, 1990; Yoshimitsu et al., 2002; Adedapo et al., 2016; Pan et al., 2020a,b). In recent years, many scholars have studied the wettability of shale (Al-Yaseri et al., 2022; Sharifigaliuk et al., 2022; Ma et al., 2022; Qin et al., 2022). Predecessors have used various

* Corresponding author. State Key Laboratory of Petroleum Resources and Prospecting, China University of Petroleum, Beijing, 102249, China.
** Corresponding author. State Key Laboratory of Petroleum Resources and Prospecting, China University of Petroleum, Beijing, 102249, China.
E-mail addresses: cjq7745@163.com (J. Chen), pangxq@cup.edu.cn (X. Pang).

https://doi.org/10.1016/j.jngse.2022.104798
Received 25 May 2022; Received in revised form 14 September 2022; Accepted 15 September 2022
Available online 20 September 2022

experimental means to study the wettability of rock-brine-CO_2; however the experimental results are different. For example, Valluri et al. (2016) used the capture-bubble method to measure the contact angle of rock-brine-crude oil, while Rego et al. (2022) evaluated the possibility of improving recovery by changing the composition of fracturing fluid to change the wettability to a wetter state. Although the main trend of wetting angle change obtained from their experimental results is the same; some of the contact angles measured by them differ by 10°. Chiquet et al. (2007) obtained from the captivity-drop technique that the brine contact angle increases with the increase in pressure. However, Stevar et al. (2019) found that when the pressure is lower than 10 MPa, the brine contact angle increases and then decreases. Yassin et al. (2017) measured the contact angle of shale samples from sedimentary basins in western Canada and found that the difference between the six different results measured by each sample was 5°–11°. The macroscopic contact angle measurement in the experiment has certain limitations and uncertainties, and the experimental cost is high. Therefore, it is necessary to study the wettability of CO_2/CH_4-brine-shale from the microscopic viewpoint (Salehi et al., 2008; Xue et al., 2015). It mainly includes the influencing factors of wettability and how these influencing factors affect the change of wettability. The influencing factors mainly include temperature, CO_2 pressure, mineralization, and the concentration ratio of CO_2 and CH_4.

Molecular dynamics (MD) is a method used in computer simulation at the atomic or molecular level of matter. It has been developing for a long time, and its application range is becoming wider (Hu et al., 2016; Pham et al., 2021). Recently, MD simulation has been developed to study the inherent contact angle of nanosolid surfaces. Yu et al. (2020) used MD to simulate the change in rock-brine-CO_2 contact angle under different temperatures and CO_2 pressure and compared the result with the experimental data; the same results were obtained, which confirmed the reliability of the molecular simulation. Although the molecular dynamics method is used to study it, the method of measuring the wetting angle is macro, which is not verified by the micro mechanism (interaction energy). Tetteh et al. (2021) simulated the effect of a cationic surfactant on the wettability of calcite using MD, revealed the molecular mechanism of wettability reversal, and provided a basis for designing effective chemical formula to enhance oil recovery. Zhou et al. (2021) used MD simulation to study the interface phenomenon in the CO_2–H_2O-kerogen system and evaluate the contact angle. The contact angle in the CO_2–H_2O-kerogen increases with increasing CO_2 pressure until it reaches 180°. Jagadisan and Heidari (2021) studied the wettability of kerogen molecules at different thermal maturity and temperatures using the MD simulation. The simulation results show that the maximum contact angle formed by type III kerogen on the surface of kerogen is 45.5°. Type II kerogen is the lowest, 20°.

The above results show that the systematic study of shale wettability, considering temperature, CO_2 pressure, salinity, and ion concentration, especially its internal interaction mechanism is unclear. Therefore, this study determines the wettability of CO_2/CH_4-brine shale at the nanoscale using MD simulation combined with the influencing factors of the wettability of the shale pore surface. First, the effects of temperature and CO_2 pressure on the wettability of organic pores in shale are studied. Subsequently, the effects of mineralization on the water contact angle were studied. And, by injecting CH_4 into CO_2, the effects of different concentration ratios of CO_2 and CH_4 on the water contact angle were studied. Finally, the order of wettability is verified by interaction energy. The research methods and results in this paper reduce the uncertainty of the experiment and are important to CS–EGR. Our experimental results not only use the wetting angle obtained during simulation to compare the wettability, but also use the interaction energy to verify the wettability, which is more accurate than the wetting angle obtained by experiments alone. This is because there will be some human operation errors and other factors in the process of the experiment, which will make the experimental results have certain deviations. The research results of this manuscript are more accurate than the experimental results and are important to CS–EGR.

2. Models and methods

2.1. Simulation principle

Alder and Wainwright, 1957 first proposed the MD, which is a method to understand the dynamic evolution of the system by analyzing the physical motion of atoms and molecules. The method is currently used after continuous exploration and improvement by later generations. The selection of potential function in MD simulation parameters is important. The potential function between atoms has developed from pair to multibody potential (Chakraborty et al., 2015; Salehi et al., 2008). In this simulation, the compass force field, which has been used in many molecular simulations involving mineral surfaces, was selected to study the interaction between atoms, (Chang et al., 2018; Heydari et al., 2021).

The function form of the compass force field is as follows (Sun, 1998; Savin and Mazo, 2020):

$$E_{total} = E_{valence} + E_{nonbond} \tag{1}$$

where E_{total} is the total energy (kcal/mol), E_{valence} is the bond energy (kcal/mol), and E_{nonbond} is the nonbond energy (kcal/mol).

$$E_{valence} = E_{bond} + E_{angle} + E_{torsion} + E_{Inversion} + E_{crossterm} \tag{2}$$

where E_{bond} is the bond-stretching energy (kcal/mol), E_{angle} is the bond angle bending energy (kcal/mol), E_{torsion} is the dihedral torsional energy (kcal/mol), $E_{\text{Inversion}}$ is the offplane interaction phase (kcal/mol), and $E_{\text{crossterm}}$ is the covalent-interaction term (kcal/mol).

The Lennard Jones potential can display the even-potential term (Jones, 1924; Sohrab et al., 2018). Therefore, nonbond energy can be written as (Al-Raeei and E-Daher, 2019; Lin et al., 2021):

$$E_{nonbond} = E_{ij} + E_{coulomb} \tag{3}$$

$$E_{ij} = \sum_{i,j} \varepsilon_{ij} \left[2\left(\frac{r_{ij}^{o}}{r_{ij}}\right)^{9} - 3\left(\frac{r_{ij}^{o}}{r_{ij}}\right)^{6} \right] \tag{4}$$

$$E_{coulomb} = \sum_{i,j} \frac{q_i q_j}{\varepsilon_o r_{ij}} \tag{5}$$

where E_{ij} is the van der Waals energy (kcal/mol), E_{coulomb} is the electrostatic interaction energy (kcal/mol), r_{ij} is the distance between particles i and j (Å), ε_{ij} is the potential well depth (kcal/mol), r_{ij}^{o} is the distance between the pairs of particles with a potential of 0 (Å), ε_0 is the dielectric constant (kcal/mol), and q_i and q_j are the charges of the particles in system (C).

2.2. Simulation process

The wettability of CO_2/CH_4-brine-shale was simulated using MD. The first step is to establish the wettability model of "CO_2-brine-shale". First create a box filled with CO_2 (80 Å × 70 Å × 78.3 Å) (Fig. 1a), a hemispherical box containing 300 water molecules (Fig. 1b), and a graphene structure with a horizontal surface (80 Å × 70 Å × 6.7 Å) (Fig. 1c). Graphene has wide application prospects in many fields due to its excellent characteristics such as high mechanical strength (Xin et al., 2015), high conductivity (El-Kady et al., 2016), high heat transfer rate (Goyal and Balandin, 2012; Li et al., 2017). Graphene itself is a two-dimensional honeycomb carbon nanomaterial, which can exhibit high chemical stability (Chi et al., 2020). When used as a thin film material, it has always occupied an important position in the field of two-dimensional materials. At present, the research and application fields of graphene mainly focus on adjusting substrate wettability (Lu et al., 2021), seawater desalination (Hegab and Zou, 2015), and

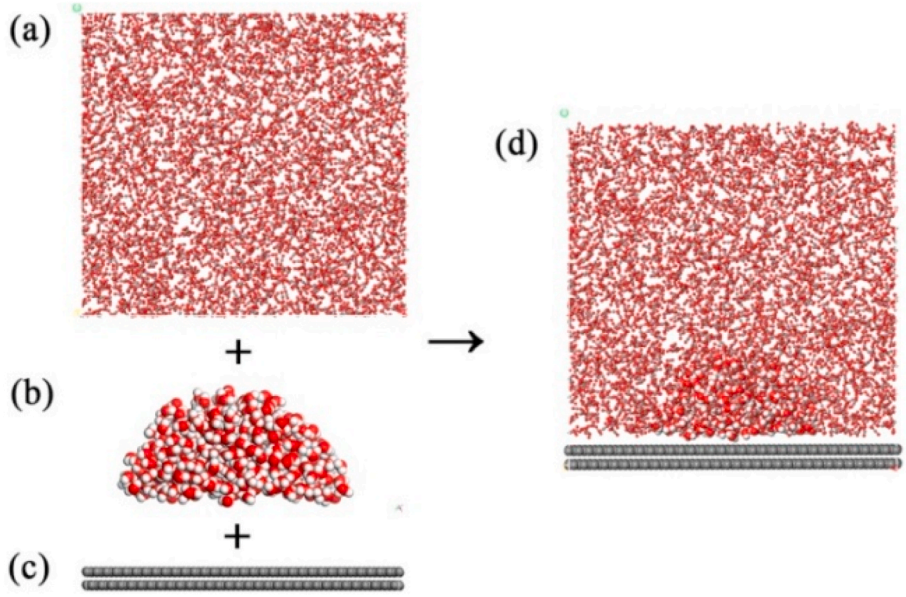

Fig. 1. Establishment process of wettability model (a. CO_2; b. Water; c. Graphene; d. Initial wettability model).

oil-water separation (Price et al., 2019). Lin et al. (2017) studied the adsorption heat, adsorption capacity and the change of adsorption capacity with temperature between shale organic matter surface and graphene surface by combining experiment and simulation, and found that graphene can be used as a good model to simulate shale organic matter surface. And, a graphene model has been successfully used to represent an organic pore surface in shale by many scholars (Bhatia et al., 2004; Tenney, 2009; Yuan et al., 2015; Lin et al., 2017). Therefore, in the simulation process, graphene surface can be used to replace the organic pore surface of shale. Then, fix the surface of graphene, relax the CO_2 and water, and optimize the structure of the CO_2 box, water box, and graphene, respectively. Optimization here refers to geometry optimization, which is usually to find the minimum point on the potential energy surface. The geometry corresponding to the minimum point is the possible equilibrium geometry of the molecule. Geometry optimization can make the molecules of the whole system reach equilibrium and stable state (Li and Chen, 2011). Finally, the optimized CO_2 box, water box, and graphene are combined into one using Materials Studio software to obtain the wettability model (Fig. 1d), and the combined wettability model is optimized. The above molecules are from the structural database of Materials Studio software. Due to the periodic influence of the simulation process, some CO_2 molecules will move to the top of the model, which is a normal phenomenon.

In the simulation process, the Andersen thermostat method is used to control the temperature (Andersen, 1980). The Ewald method with high accuracy is used to calculate electrostatic interactions (Zhong et al., 2013). The steepest descent methods optimized the structure of the initial model (Chang et al., 2018). The van der Waals interaction is calculated using the atom-based method (Xia et al., 2016). The main parameters in the simulation process are shown in Table 1. To ensure the accuracy of the simulation, the fixed-time step of all simulations is 1 fs (Zhu et al., 2015).

2.3. Wetting angle measurement

With the continuous development of molecular dynamics in wettability measurement, many methods have emerged to measure the wetting angle (Bhattacharjee and Khan, 2019; Le and Walsh, 2021; Dong et al., 2021). In this study, the most commonly used geometric method was used to calculate the contact (Feng and Tahir, 1995; Li and Wang, 2017). In order to make the experimental results more accurate, the measurement result is the average value of the wetting angle obtained at the last time of three simulations (1000ps). The principle is as follows: when the mineral interface is hydrophilic or hydrophobic, the contact angle between the corresponding droplet and interface is an acute (Fig. 2a) or obtuse (Fig. 2b) angle, respectively, which meets the following formula:

$$\cos\theta = 1 - \frac{h}{R} \tag{6}$$

$$(R-h)^2 + r^2 = R^2 \tag{7}$$

where h represents the height from the center point of the liquid circle to the surface of solid minerals, and R represents the radius of the ball corresponding to the droplet.

Table 1
Main input parameters of different modules in the simulation process.

Simulation Modules	Parameter	Input	Unit
Amorphous Cell-Packing	Density of CO_2 box	0.6	g/cm^3
	Density of H_2O box	1.0	g/cm^3
	Loading steps	1000	/
Geometry Optimization	Maximum number of iterations	500	/
	Algorithm	Steepest descent	/
Dynamics	Time step	1	fs
	Density of the whole system	0.729	g/cm^3
	Ensemble	NVT	/
	Total simulation time	1000	ps
	Cut-off distance	12.5	Å
	Number of steps	1,000,000	/
	Thermostat	Andersen	/
	Initial velocities	Random	/

3. Results

3.1. Effect of temperature on water contact angle

We simulated the variation characteristics of wettability at 298 K, 313 K, 323 K, and 343 K under a certain pressure using the MD and

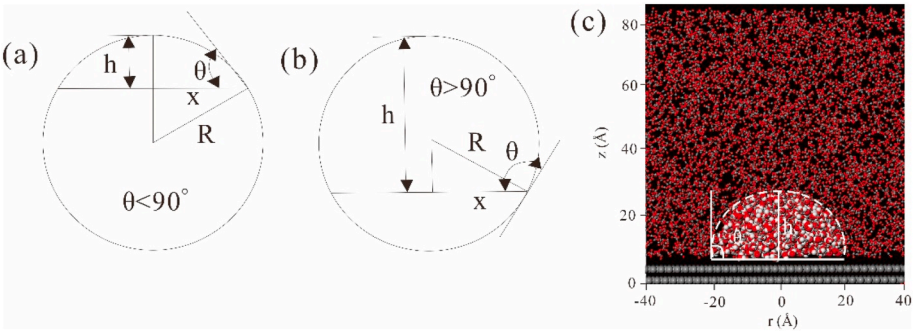

Fig. 2. Schematic of contact angle calculation (a. Acute angle; b. Obtuse angle; c. Stereogram).

calculated the wetting angle at each pressure and temperature using the geometric method (Fig. 3). We have compared the simulated data with the experimental data in organic-rich shale because there is no data on the water contact angle of the graphene surface in carbon dioxide. The reasons for this feasibility and some differences will be introduced in the section of 4.5.

Under certain pressure, the contact angle decreases with the increase in temperature, indicating that the water wettability increases with the increase in temperature (Fig. 3). This is consistent with the conclusion of Li and Xiao, 2012 using quantum mechanical simulation to study the wetting of nanodroplets on the graphene. When the CO_2 pressure is 20 MPa and the temperature is 298 K and 313 K because there is no distribution of water on the graphene, the contact angle is 180°, indicating complete CO_2 wetting. When the CO_2 pressure is 5 MPa and the temperature is higher than the supercritical temperature, water is neutrally wetted on the graphene surface, and when it is lower than 298 K, water is CO_2 wetted on the graphene surface (Fig. 4). When the CO_2 pressure is 10 and 20 MPa, water is wetted by CO_2 on the surface of graphene. This is consistent with the conclusion reached by Yu et al. (2020) using the MD. Finally, the water contact angle results calculated using the MD simulation are compared with the experimental results of others (Pan et al., 2018) (Fig. 4). We found that the difference between our simulation results and previous experimental results was very small, which verified the accuracy of our simulation results.

In this study, the relationship between different wetting degrees, corresponding to different contact angles, adopts the classification proposed by Fanchi (2005), which is that 0°–75° is water wetting, 75°–105° is neutral wetting, and 105°–180° is CO_2 wetting. Thomas Andrews measured two critical parameters of carbon dioxide in 1869: the supercritical pressure was 7.2 MPa and the supercritical temperature

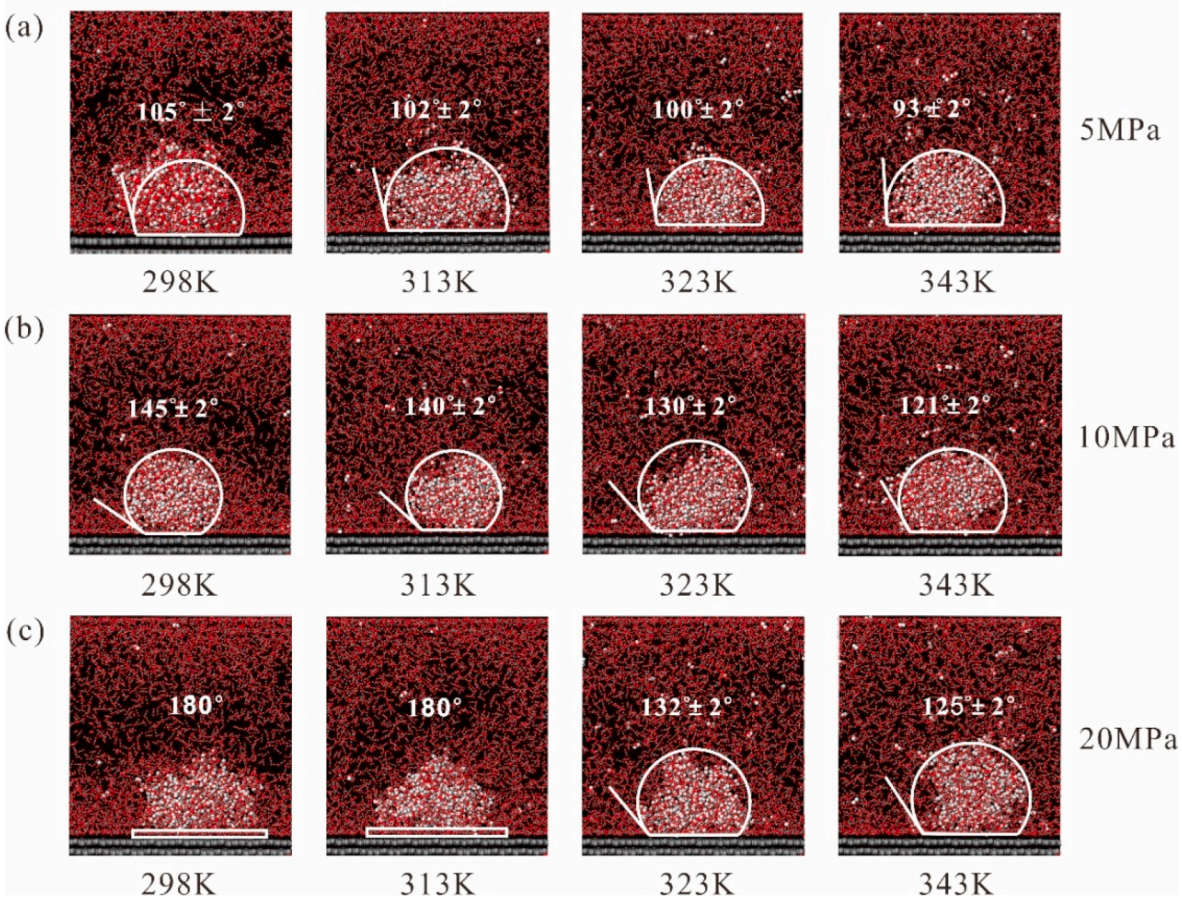

Fig. 3. Variation of contact angle on graphene at different temperatures and pressures.

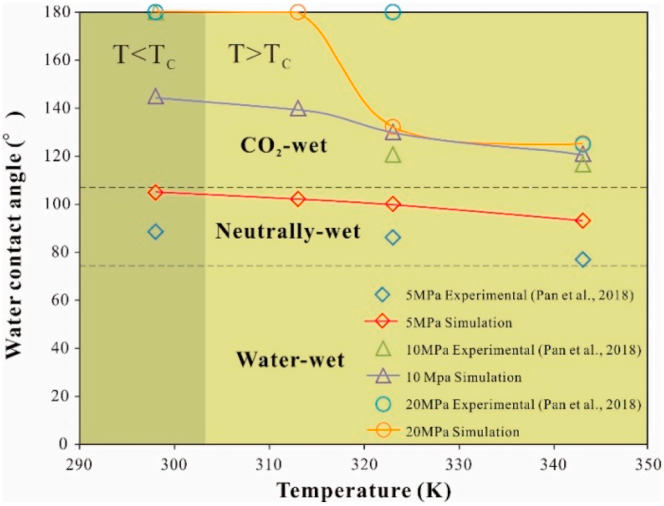

Fig. 4. Comparison of contact angle changes on graphene obtained using experiment and simulation at different temperatures.

was 304.065 K. Their recognized values in 2013 were 7.375 MPa and 303.05 K, respectively (Lou and Chen, 2013; Yu, 2014).

3.2. Effect of CO_2 pressure on water contact angles

At a fixed temperature, with the increase in CO_2 pressure, the contact angle of water on the surface of graphene increases, indicating that its water wettability decreases (Fig. 3). When the critical pressure is lower than 7.375 MPa, the water is neutral wetted on the surface of graphene at 298 K, 313 K, 323 K, and 343 K (Fig. 5). When the critical pressure is higher than 7.375 MPa, water at different temperatures is wetted by CO_2 on the surface of graphene, and the wettability reversal occurs. This shows that supercritical conditions determine wettability. This conclusion has the same trend as the conclusion reached by Pan et al., 2019 through experiment.

3.3. Effects of mineralization on water contact angle

The effects of mineralization on the water contact angle of graphene were studied by studying NaCl, $CaCl_2$, and $MgCl_2$ solutions using concentrations of 1%, 3%, and 5%. The setting temperature of this

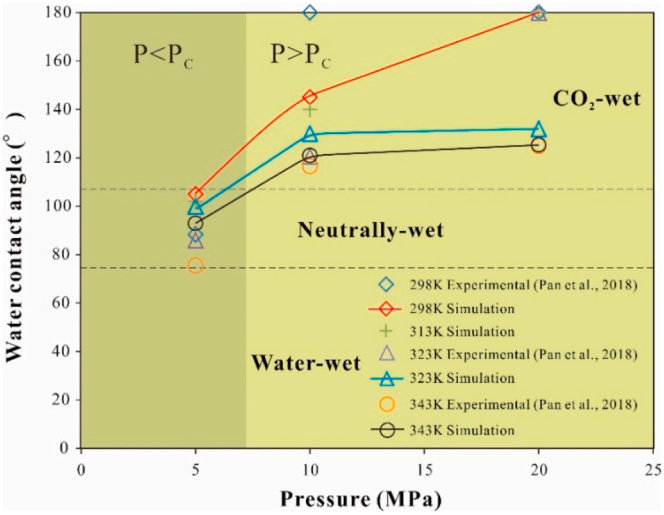

Fig. 5. Comparison of contact angle changes on graphene obtained using experiment and simulation under different pressures.

simulation is 323 K, and the pressure is 5 MPa. Fig. 6 shows that for NaCl solutions with concentrations of 1%, 3%, and 5%, the contact angles are 102° ± 2°, 108° ± 2°, and 113° ± 2°, respectively. With the increase in solution salinity, the contact angle increases, and the water wettability decreases. In addition, with the increase in salinity, the water contact angle of $CaCl_2$ and $MgCl_2$ solutions on the surface of graphene increases, and the water wettability decreases (Fig. 7). Simultaneously, with the increase in solution salinity, the density of water molecules on the surface of graphene decreases, and the water wettability decreases (Fig. 8). This is the same as the results obtained by Yu et al. (2021) through MD simulation.

The ion concentration affects the water contact angle of the graphene surface (Fig. 7). From the slope of each curve in Fig. 7, with the increase of ion concentration in solutions containing different ion types, the order of change of amplitude of contact angle is $MgCl_2$ > $CaCl_2$ > NaCl, indicating that divalent cations (Mg^{2+} and Ca^{2+}) affect the wetting angle than monovalent cations (Na^+) under the same concentration of droplets. In addition, Fig. 8 shows that ions gather inside the droplet and are not directly adsorbed on the surface of graphene. Mg^{2+} are closer to the surface than Na^+ and Ca^{2+}, indicating that the adsorption capacity of Mg^{2+} on graphene is stronger than Na^+ and Ca^{2+}, which is consistent with the previous conclusions obtained using Zeta potential experiment (Kasha et al., 2015; Jackson et al., 2016).

3.4. Effect of concentration ratio of CO_2 and CH_4 on water contact angles

In the shale reservoir containing CO_2 and CH_4 gas, the wettability of rocks is important for CS–EGR (Li et al., 2018; Dong et al., 2022). The effects of different concentration ratios on water contact angles were studied by changing the concentration ratio of CO_2 and CH_4. The setting temperature of this simulation is 323 K, and the pressure is 5 MPa.

Figs. 9 and 10 show that the water contact angle decreases with the decrease in CO_2 content in the system. The water wettability increases with the increase in CH_4 content, and they are all neutral wettability. This is the same as the conclusion by Pan et al. (2018) that the contact angle of water in the CH_4-shale system is lower than that of CO_2-shale. We found that CO_2 and CH_4 molecules are distributed on the solid surface of graphene and show a multilayer adsorption state (Fig. 11). The relative concentration of CO_2 adsorbed on the first layer of graphene surface is large, which is about 2.4 times that of CH_4 adsorbed on the first layer of graphene surface, indicating that the graphene surface has a strong adsorption capacity for CO_2. This is consistent with the previous conclusion that because of the smaller molecular diameter and higher adsorption energy of CO_2, the adsorption ratio of CO_2 to CH_4 is about 2:1 (Gentzis, 2000; Guan et al., 2018). With the decrease in CO_2 ratio, the relative concentration of CO_2 on the surface of graphene decreases (Fig. 11a). In addition, with the decrease in the CH_4 ratio, the relative concentration of CH_4 on the surface of graphene decreases (Fig. 11b).

4. Discussion

4.1. Stability

The internal energy of the system is composed of kinetic energy and potential energy. Among them, kinetic energy is generally used to characterize the equilibrium state of the system (Zhong et al., 2013; Chang et al., 2018). The evolution of kinetic energy in the wettability models at different temperatures is shown in Fig. 12. After 8 ps, the kinetic energy maintains a stable state (Fig. 12), indicating that the simulation time is long enough to keep the studied system stable.

4.2. Mean square displacement (MSD) and self-diffusion coefficient (D)

The movement characteristics of water molecules on the mineral surface are analyzed by calculating the MSD and D (Wang et al., 2015; Tirjoo et al., 2019; Amirhossein et al., 2021).

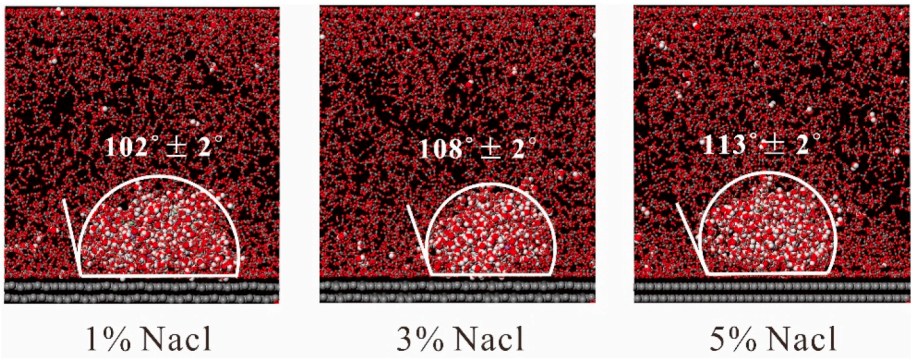

Fig. 6. Change of water contact angle at different concentrations of NaCl solution on a graphene surface.

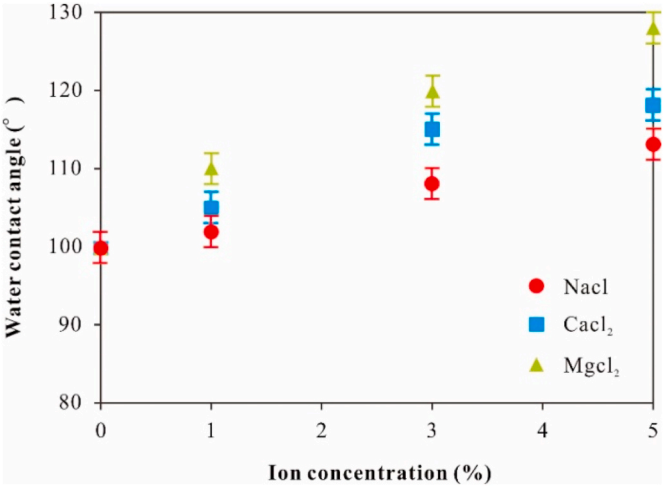

Fig. 7. Relationship between the type and content of ions and the change of water contact angle.

$$MSD = \frac{1}{N}\sum_{i=1}^{N}[r_i(t) - r_i(0)]^2 \tag{8}$$

$$D = \frac{1}{6N}\lim_{t\to\infty}\frac{d}{dt}\sum_{i=1}^{N}[r_i(t) - r_i(0)]^2 = \frac{1}{6}K_{MSD} \tag{9}$$

where N is the number of diffusion molecules, $r(t)$ and $r(0)$ are the position vectors of molecules at t and $t = 0$, respectively, K_{MSD} is the slope of the MSD curve.

With the increase in simulation time, the value of MSD increases; however, its slope decreases, and there are two slopes in general (Fig. 13). This is because some water molecules at the early stage of simulation are adsorbed to the surface of graphene, and the adsorption capacity of graphene for water is large; thus, the self-diffusion coefficient is high. In the later stage, only a small part of water molecules suspended in CO_2 continues to diffuse, and the natural self-diffusion coefficient is small. According to formula (9), the D of water molecules is 343 K > 323 K > 313 K > 298 K. The fluidity of water molecules has a certain relationship with the temperature change. The higher the temperature, the greater the self-diffusion coefficient, which is the same result drawn by Zhao and Jin (2020) through MD simulation. The higher the temperature, the faster and stronger the adsorption of water on the graphene, resulting in increased self-diffusion and better separation of oil from the graphene surface (Amirhossein et al., 2021).

4.3. Interaction energy

To understand the wetting mechanism from the microscopic viewpoint, we take the last moment of MD simulation (1000 ps) and calculated the interaction energy between CO_2/water and graphene at different temperatures and different pressures (Fig. 14). The interaction energy ($E_{C\text{-}S}$) between CO_2 molecule and graphene can be defined as (Chang et al., 2018; Ma et al., 2019):

$$E_{C-S} = E_{C+S} - E_C - E_S \tag{10}$$

where E_{C+S} is the total energy of the CO_2 molecule and graphene, kcal/mol; E_C is the energy of the CO_2 molecule, kcal/mol; E_S is the energy of graphene, kcal/mol.

Similarly, the interaction energy ($E_{W\text{-}S}$) between water molecules and graphene can be defined as the following:

$$E_{W-S} = E_{W+S} - E_W - E_S \tag{11}$$

where E_{W+S} is the total energy of water molecules and graphene, kcal/mol; E_W is the energy of water molecules, kcal/mol.

The interaction energy between $E_{C\text{-}S}$ and $E_{W\text{-}S}$ (ΔE):

$$\Delta E = E_{C-S} - E_{W-S} \tag{12}$$

Studies show that when ΔE is negative, the rock surface is wetted by CO_2 (Chang et al., 2018; Zhong et al., 2013). Therefore, the water molecules on graphene are easily replaced by CO_2 molecules. Fig. 14 shows the difference in interaction energy between the CO_2 molecules and water and graphene surfaces at different temperatures and different pressures (ΔE). The ΔE is negative, indicating that the interaction energy between the CO_2 molecule and graphene is greater than that between the water molecule and graphene, and the graphene surface is wetted by CO_2. In addition, with the increase in temperature, the interaction energy between $E_{C\text{-}S}$ and $E_{W\text{-}S}$ is (ΔE) is smaller, indicating that its CO_2 wettability is weaker, and water wettability is stronger, which is the same result drawn in the section of 3.1 (Fig. 14a). With the increase in pressure, the interaction energy between $E_{C\text{-}S}$ and $E_{W\text{-}S}$ is (ΔE) is bigger, indicating that its CO_2 wettability is stronger, and water wettability is weaker, which is the same result drawn in the section of 3.2 (Fig. 14b). We can observe that the value of ΔE does not change greatly (Fig. 14), because the change of contact angle corresponding to different ΔE is also small. At the temperature of 298–343 K, the wetting angle changes by 12°. The above discussion shows the difference between $E_{C\text{-}S}$ and $E_{W\text{-}S}$ (ΔE). The different wettability of the graphene surface can be explained.

4.4. Effect of clay minerals in shale on wettability

Shale is a mixture of various inorganic minerals and organic matter (Loucks et al., 2012), and its structure and heterogeneity will affect its wettability. The surface of organic matter is generally considered hydrophobic, while inorganic minerals (especially clay minerals) tend to

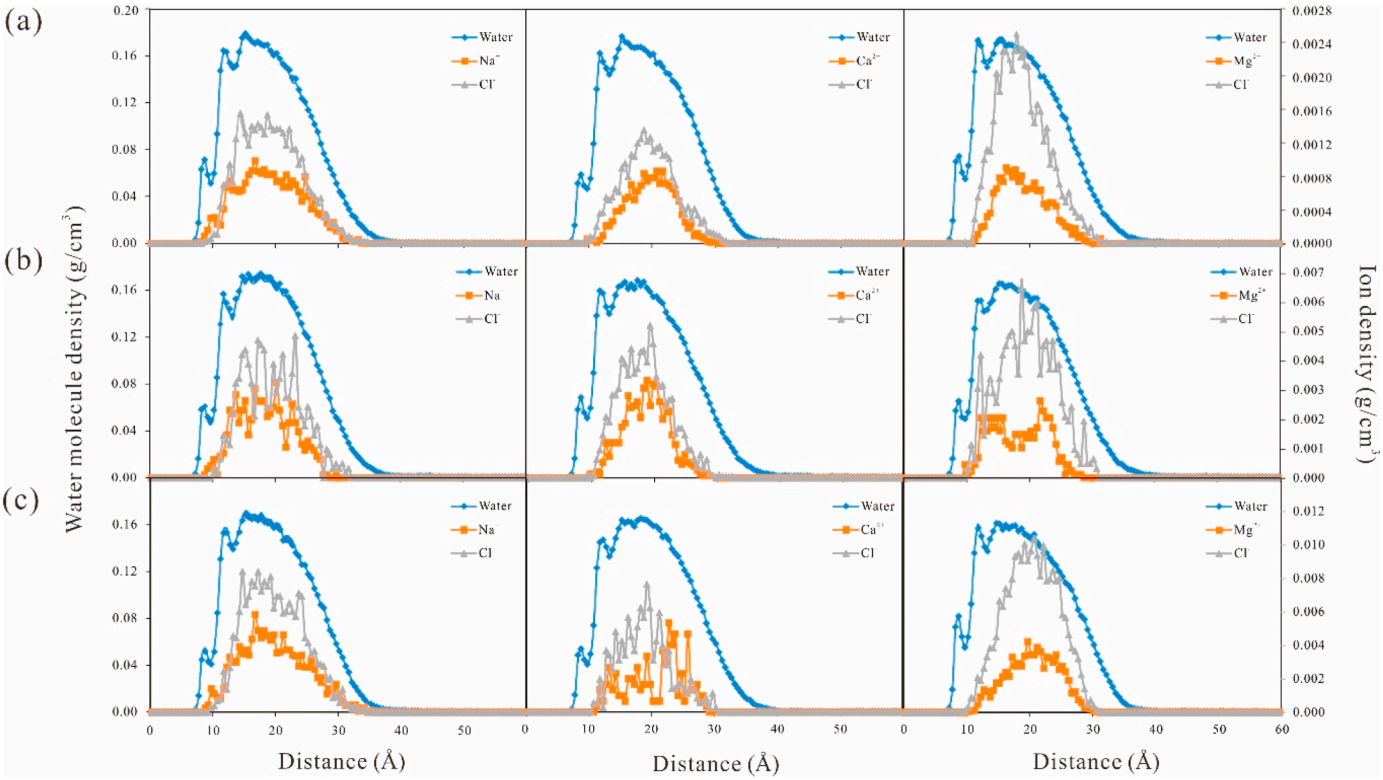

Fig. 8. Density distribution of water molecules and ions along the z-axis of solutions containing different ion types (a. Concentration is 1% solution; b. Concentration is 3% solution; c. Concentration is 5% solution).

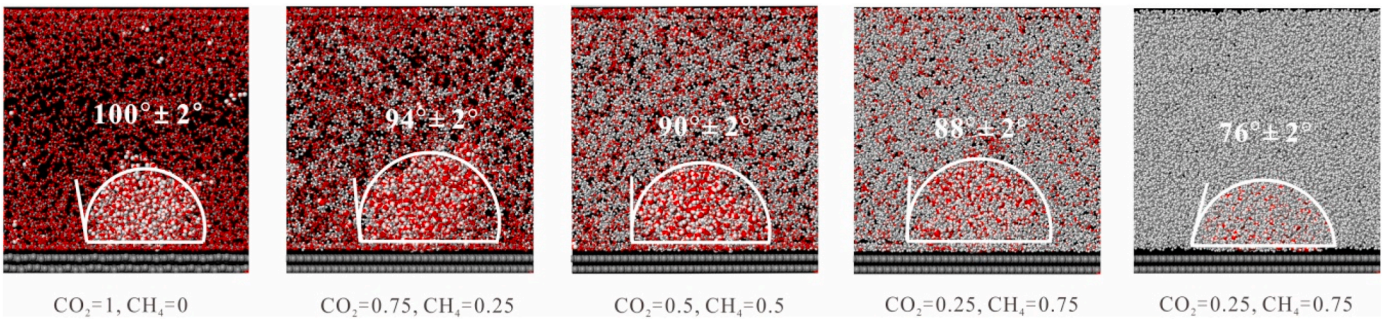

Fig. 9. Changes of water contact angle under different CO_2 and CH_4 concentration ratios.

be hydrophilic (Jin and Firoozabadi, 2014). Shale with different minerals has different affinity for water, ranging from hydrophilicity to hydrophobicity, that is, they show mixed wettability (Alhammadi et al., 2017), which makes it more challenging to describe their wetting behavior. For example, the wettability of shale with relatively high clay content is not constant and will change continuously during the hydration/permeability process related to clay.

Siddiqui et al. (2018) found that the contact angle of oil and water increased with the increase of clay content. However, when using high salinity solutions, the contact angle decreases with the increase of clay content (Sayyouh et al., 1990). Li et al. (2021) showed by experimental means that clay minerals (type and content) may be the most important factor affecting the wettability of shale. Specifically, the contents of illite and illite/smectite mixed layer are positively and negatively correlated with calcium, respectively, indicating that illite tends to be hydrophobic, while illite/smectite mixed layer is more hydrophilic. However, Fauziah et al. (2018) showed that hydrophilic shale is rich in illite. Li et al. (2021) believed that the weak affinity of illite for water may be due to the asphaltene on its surface. In addition, with the increase of kaolinite and chlorite content, the contact angle first decreased, and then increased rapidly. This may be attributed to the hydrophobicity of asphalt containing kaolinite and chlorite.

4.5. *Effect on CS–EGR*

From the above discussion, we know that when the pressure increases above the critical pressure value (7.375 MPa) or the temperature decreases, the CO_2 in the system becomes wetter, indicating that the interaction between CO_2 and shale is stronger (Chiquet et al., 2007). Huang et al. (2018) found that the adsorption capacity of organic matter on the surface of shale was the largest when the gas pressure increased to the critical pressure (7.375 MPa). With the continuous increase in pressure, the adsorption capacity tends to be stable. Subsequent experiments proved that this phenomenon is caused by the affinity between CO_2 and organic matter in shale. This affinity contributes to CO_2 storage and improves the adsorption capacity of CO_2. At the early stages, higher pressures should be used. When the pressure rises to 7.375 MPa, the output of CH_4 tends to be stable and the storage capacity of CO_2 reaches

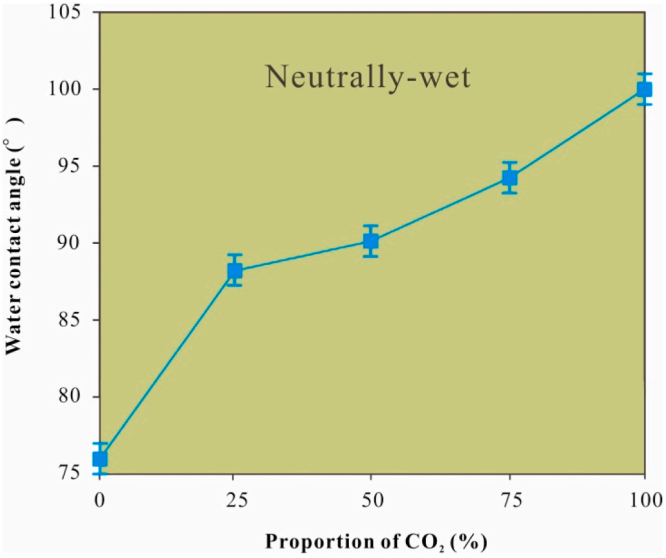

Fig. 10. Relationship between the concentration ratio of different CO_2 and CH_4 and the change of water contact angle.

the maximum. Moreover, the capture safety and storage capacity should be considered when determining the pressure.

The contact angle of water in the CH_4-shale system is lower than that of the CO_2-shale. This shows that the adsorption capacity of CO_2 for organic matter is higher than that of CH_4. This is because, at low pressure, the adsorption sites with strong energy are occupied by the CO_2 molecules. With the increase in pressure, once the higher energy parts are filled, carbon dioxide and methane begin to occupy the low-energy areas (Huang et al., 2018).

Therefore, on the surface of graphene, the adsorption capacity of CO_2 is larger; the area is wider, and the emission of CH_4 is increased. In addition, we can improve the CS–EGR purpose by improving CO_2 injection time, volume, and injection because the adsorption of organic matter on the surface is affected by temperature, pressure, TOC, etc (Guan et al., 2018; Arif et al., 2016).

4.6. Limitations of MD simulation

It is mentioned in 3.1 that the effect of temperature on the contact angle change trend is consistent; however, there is a difference between the molecular-dynamic simulation and experimental results. The contact angle we simulated is larger than that obtained from the experiment. This is because, in this study, we used graphene to replace the surface of organic matter. The TOC content of graphene is 100%; whereas, the TOC content of the shale sample in the experiment is lower. High TOC content in shale will increase the water contact angle (Hu, 2014; Hu et al., 2016). Moreover, the surface roughness of graphene will cause measurement error of water contact angle, and even lead to the transition from hydrophilicity to hydrophobicity. For example, Lan et al. (2015) tested the contact angle value of water and oil with fresh core plugs, and found that the oil completely diffused to the surface, which was quite different from the result of the water-air contact angle value (37° - 73°) measured in the experiment. Therefore, if the actual mineral surface roughness is considered, different results should be obtained. Generally, if the mineral composition is uniform, the contact angle value increases with the decrease of roughness. However, the graphene surface in MD

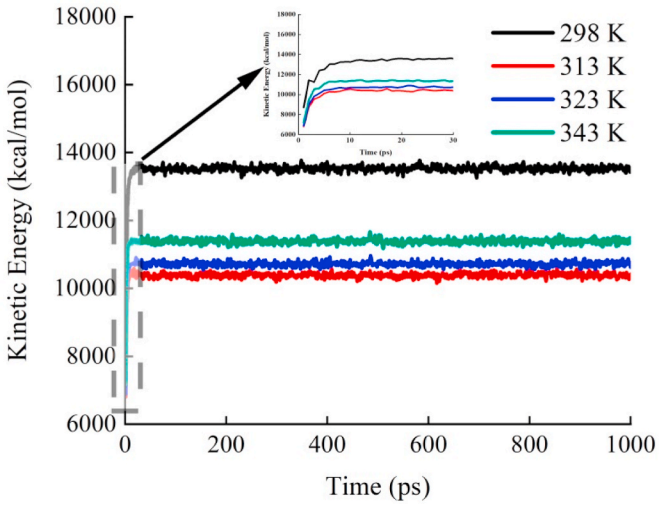

Fig. 12. Variation diagram of kinetic energy in wettability model at different temperatures at 5 MPa.

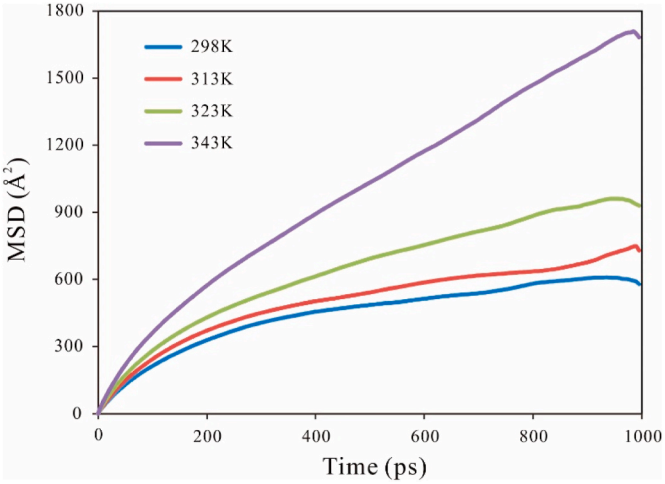

Fig. 13. Variation curve of mean square displacement of water molecules on graphene surface at different temperatures under 5 MPa.

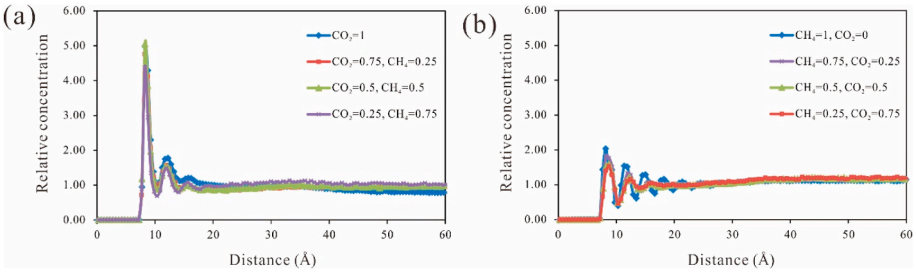

Fig. 11. Relative concentration of CO_2/CH_4 on graphene surface under different concentration ratios of CO_2 and CH_4 (a. Molecular number of CO_2; b. Molecular number of CH_4).

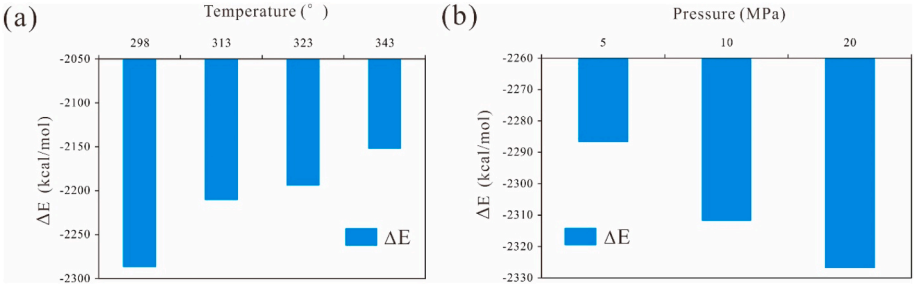

Fig. 14. Difference of interaction energy between CO_2 molecule and water and graphene surface (a. Different temperatures; b. Different pressures).

simulation does not consider the effect of surface roughness.

Therefore, these influencing factors are important in the study of reservoir wettability. In our future research, we will establish a real organic matter surface, which will have a realistic TOC content and a certain roughness, close to the shale rich in organic matter.

5. Conclusions

In this study, we used MD simulation to study the wettability of CO_2/CH_4-graphene-water/Brine under reservoir conditions. It mainly includes the influencing factors of wettability and how these influencing factors affect the change of wettability. The effects of temperature, pressure, mineralization, and concentration ratio of CO_2 and CH_4 on water contact angle are considered, the order of wettability was verified by interaction energy, and the significance of CS–EGR is clarified. The main conclusions are as follows:

(1) Under certain pressures, the water wettability increases with the increase in temperature. When the CO_2 pressure is 5 MPa and the temperature is higher than the supercritical temperature, water is neutrally wetted on the surface of graphene. Below 298 K, water is wetted by CO_2 on the surface of graphene.
(2) The contact angle of graphene decreases with the increase in water pressure. Below the critical pressure of 7.375 MPa, water at different temperatures is neutrally wetted on the surface of graphene. When the critical pressure is higher than 7.375 MPa, water at different temperatures is wetted by CO_2 on the surface of graphene, and the wettability reversal occurs.
(3) With the increase in solution salinity, the contact angle increases, and the water wettability decreases. The ion concentration affects the water contact angle. At the same concentration of droplets, divalent cations (Mg^{2+} and Ca^{2+}) affect the wetting angle more than monovalent cations (Na^{+}). The adsorption capacity of Mg^{2+} on the graphene surface is stronger than that of Na^{+} and Ca^{2+}.
(4) The water contact angle decreases with the decrease in CO_2 content in the system. The water wettability increases with the increase in CH_4 content, and they are all neutral wettability. The adsorption capacity of the graphene surface for CO_2 is stronger than that of CH_4. Therefore, CO_2 injection can improve the displacement efficiency of CH_4 and improve natural gas recovery.
(5) The adsorption of organic matter on the surface is affected by temperature, pressure, TOC, etc. CO_2 injection timing, injection volume, and injection temperature can be optimized to improve gas displacement efficiency. When determining the pressure, the capture safety and storage capacity should be considered.

Credit author statement

Kanyuan Shi: Investigation, Methodology, Formal analysis, Data curation, Writing – original draft. **Junqing Chen:** Conceptualization, Methodology, Writing – review & editing, Supervision, Validation, Funding acquisition. **Xiongqi Pang:** Methodology, Visualization, Writing – review & editing. **Fujie Jiang:** Methodology, Visualization, Writing – review & editing. **Shasha Hui:** Supervision, Methodology, Writing – review & editing. **Hong Pang:** Supervision, Methodology, Writing – review & editing. **Kuiyou Ma:** Supervision, Methodology, Writing – review & editing. **Qi Cong:** Supervision, Methodology, Writing – review & editing.

Declaration of competing interest

The authors declare that they have no known competing financial interests or personal relationships that could have appeared to influence the work reported in this paper.

Data availability

No data was used for the research described in the article.

Acknowledgements

This work was supported by the National Natural Science Foundation of China (grant number 42102145, 41872148); the Science Foundation of China University of Petroleum, Beijing (grant number 2462020BJRC005, 2462022YXZZ007); the major science and technology projects of CNPC during the “14th five-year plan” (grant number 2021DJ0101); and the Joint Fund of the National Natural Science Foundation of China (grant number U19B6003-02-04).

References

Adedapo, A., Sarma, H., Alsumaiti, A., 2016. An experimental investigation into the impact of sulfate ions in smart water to improve oil recovery in carbonate reservoirs. Transport Porous Media 111, 649–668. https://doi.org/10.1007/s11242-015-0616-4.

Ajayi, T., Gomes, J.S., Bera, A., 2019. A review of CO2 storage in geological formations emphasizing modeling, monitoring and capacity estimation approaches. Petrol. Sci. 16, 1028–1063. https://doi.org/10.1007/s12182-019-0340-8.

Al-Raeei, M., E-Daher, M.S., 2019. A numerical method for fractional Schrdinger equation of Lennard-Jones potential. Phys. Lett. 383, 125831 https://doi.org/10.1016/j.physleta.2019.07.019.

Al-Yaseri, A., Yekeen, N., Mahmoud, M., Kakati, A., Xie, Q., Giwelli, A., 2022. Thermodynamic characterization of H2-brine-shale wettability: implications for hydrogen storage at subsurface. Int. J. Hydrogen Energy 47, 22510–22521. https://doi.org/10.1016/j.ijhydene.2022.05.086.

Alder, B.J., Wainwright, T.E., 1957. Phase transition for a hard sphere system. J. Chem. Phys. 27, 1208–1209. https://doi.org/10.1063/1.1743957.

Alhammadi, A.M., AlRatrout, A., Singh, K., Bijeljic, B., Blunt, M.J., 2017. In situ characterization of mixed-wettability in a reservoir rock at subsurface conditions. Sci. Rep. 7, 1–9. https://doi.org/10.1038/s41598-017-10992-w.

Amirhossein, F.F., Abdolnabi, H., Ghasem, Z., Tamsilian, Y., 2021. Molecular dynamics modeling and simulation of silicon dioxide-low salinity water nanofluid for enhanced oil recovery. J. Mol. Liq. 339, 116834 https://doi.org/10.1016/j.molliq.2021.116834.

Andersen, H.C., 1980. Molecular dynamics simulations at constant pressure and/or temperature. J. Chem. Phys. 72, 2384–2393. https://doi.org/10.1063/1.439486.

Arif, M., Barifcani, A., Lebedev, M., Lglauer, S., 2016. CO2-wettability of low to high rank coal seams: implications for carbon sequestration and enhanced methane recovery. Fuel 181, 680–689. https://doi.org/10.1016/j.fuel.2016.05.053.

Belhaj, H., Abukhalifeh, H., Javid, K., 2013. Miscible oil recovery utilizing N2 and/or HC gases in CO2 injection. J. Pet. Sci. Eng. 111, 144–152. https://doi.org/10.1016/j.petrol.2013.08.030.

Bhatia, S.K., Tran, K., Nguyen, T.X., Nicholson, D., 2004. High-pressure adsorption capacity and structure of CO2 in carbon slit pores: theory and simulation. Langmuir 20, 9612–9620. https://doi.org/10.1021/la048571i.
Bhattacharjee, S., Khan, S., 2019. Effect of alkyl chain length on the wetting behavior of imidazolium based ionic liquids: a molecular dynamics study. Fluid Phase Equil. 501, 112253 https://doi.org/10.1016/j.fluid.2019.112253.
Birkholzer, J.T., Oldenburg, C.M., Zhou, Q.L., 2015. CO2 migration and pressure evolution in deep saline aquifers. Int. J. Greenh. Gas Control 40, 203–220. https://doi.org/10.1016/j.ijggc.2015.03.022.
Chakraborty, T., Hens, A., Kulashrestha, S., Murmu, N.C., Banerjee, P., 2015. Calculation of diffusion coefficient of long chain molecules using molecular dynamics. Physica. E. 69, 371–377. https://doi.org/10.1016/j.physe.2015.01.008.
Chang, X., Xue, Q.Z., Li, X.F., Zhang, J.Q., Zhu, L., He, D.L., Zheng, H.X., Lu, S.F., Liu, Z. L., 2018. Inherent wettability of different rock surfaces at nanoscale: a theoretical study. Appl. Surf. Sci. 434, 73–81. https://doi.org/10.1016/j.apsusc.2017.10.173.
Chi, Y.S., Chong, J.Y., Wang, B., Li, K., 2020. Pristine graphene membranes supported on ceramic hollow fibre prepared via a sacrificial layer assisted CVD approach. J. Membr. Sci. 595, 117479 https://doi.org/10.1016/j.memsci.2019.117479.
Chiquet, P., Broseta, D., Thibeau, S., 2007. Wettability alteration of caprock minerals by carbon dioxide. Geofluids 7, 112–122. https://doi.org/10.1111/j.1468-8123.2007.00168.x.
Dong, H., Zhou, Y., Zheng, C., Zhou, J.P., 2021. On the role of the amphiphobic surface properties in droplet wetting behaviors via molecular dynamics simulation. Appl. Surf. Sci. 544, 148916 https://doi.org/10.1016/j.apsusc.2020.148916.
Dong, M.Z., Gong, H.J., Sang, Q., Zhao, X.Y., Zhu, C.F., 2022. Review of CO2-kerogen interaction and its effects on enhanced oil recovery and carbon sequestration in shale oil reservoirs. Resources Chemicals and Materials 1, 93–113. https://doi.org/10.1016/j.recm.2022.01.006.
El-Kady, M.F., Shao, Y., Kaner, R.B., 2016. Graphene for batteries, supercapacitors and beyond. Nat. Rev. Mater. 1, 16033 https://doi.org/10.1038/natrevmats.2016.33.
Famoori, F., Azin, R., Osfouri, S., Arya, N., 2021. Experimental investigation of the geochemical and mineralogical interaction between CO2 and carbonate: evaluation of CO2 sequestration in dolomite-calcite formations. Ene. Cli. Cha. 2, 100029 https://doi.org/10.1016/j.egycc.2021.100029.
Fan, C.J., Elsworth, C., Li, S., Zhou, L.J., Yang, Z.H., Song, Y., 2019. Thermo-hydro-mechanical-chemical couplings controlling CH4 production and CO2 sequestration in enhanced coalbed methane recovery. Energy 173, 1054–1077. https://doi.org/10.1016/j.energy.2019.02.126.
Fanchi, J.R., 2005. Principles of Applied Reservoir Simulation. Elsevier.
Fauziah, C.A., Al-Yaseri, A.Z., Beloborodov, R., Siddiqui, M.A., Lebedev, M., Parsons, D., 2018. Carbon dioxide/brine, nitrogen/brine, and oil/brine wettability of montmorillonite, illite, and kaolinite at elevated pressure and temperature. Energy Fuel. 33, 441–448. https://doi.org/10.1021/acs.energyfuels.8b02845.
Feng, F.C., Tahir, C., 1995. Wetting of crystalline polymer surfaces: a molecular dynamics simulation. J. Chem. Phys. 103 https://doi.org/10.1063/1.470016, 9053-9053.
Feng, Q.Q., Qiu, N.S., Borjigin, T., Wu, H., Zhang, J.T., Shen, B.J., Wang, J.S., 2022. Tectonic evolution revealed by thermo-kinematic and its effect on shale gas preservation. Energy 240, 122781. https://doi.org/10.1016/j.energy.2021.122781.
Ge, X., Guo, T.L., Ma, Y.S., Wang, G.L., Li, M.W., Zhao, P.R., Yu, X.Q., Li, S.G., Fan, H.J., Zhao, T., 2022. Fracture development and inter-well interference for shale gas production from the Wufeng-Longmaxi Formation in a gentle syncline area of Weirong shale gas field, southern Sichuan, China. J. Petrol. Sci. Eng. 212, 110207 https://doi.org/10.1016/j.petrol.2022.110207.
Gentzis, T., 2000. Subsurface sequestration of carbon dioxide — an overview from an Alberta (Canada) perspective. Int. J. Coal Geol. 43, 287–305. https://doi.org/10.1016/S0166-5162(99)00064-6.
Goyal, V., Balandin, A.A., 2012. Thermal properties of the hybrid graphene-metal nano micro-composites: applications in thermal interface materials. Appl. Phys. Lett. 100, 073113 https://doi.org/10.1016/j.ssc.2012.04.034.
Guan, C., Liu, S., Li, C.W., Wang, Y., Zhao, Y.X., 2018. The temperature effect on the methane and CO2 adsorption capacities of Illinois coal. Fuel 211, 241–250. https://doi.org/10.1016/j.fuel.2017.09.046.
Hegab, H.M., Zou, L.D., 2015. Graphene oxide-assisted membranes: fabrication and potential applications in desalination and water purification. J. Membr. Sci. 484, 95–106. https://doi.org/10.1016/j.memsci.2015.03.011.
Heydari, M., Sharif, F., Ebrahimi, M., 2021. A molecular dynamics study on the role of oxygen-containing functional groups on the adhesion of polymeric films to the aluminum surface. Fluid Phase Equil. 536, 112966 https://doi.org/10.1016/j.fluid.2021.112966.
Hu, Y.N., 2014. Dependence of organic pore wettability on kerogen maturity: a water droplet microscopic simulation study. SPE. Annu. Tech. Conf. Exhib. 7, 5621–5632. https://doi.org/10.2118/173476-stu.
Hu, Y.N., Devegowda, D., Sigal, R., 2016. A microscopic characterization of wettability in shale kerogen with varying maturity levels. J. Nat. Gas Sci. Eng. 33, 1078–1086. https://doi.org/10.1016/j.jngse.2016.06.014.
Hu, T., Pang, X.Q., Jiang, S., Wang, Q.F., Zheng, X.W., Ding, X.G., Zhao, Y., Zhu, C.X., Li, H., 2018. Oil content evaluation of lacustrine organic-rich shale with strong heterogeneity: a case study of the Middle Permian Lucaogou Formation in Jimusaer Sag, Junggar Basin, NW China. Fuel 221, 196–205. https://doi.org/10.1016/j.fuel.2018.02.082.
Huang, L., Ning, Z., Wang, Q., Qi, R.R., Cheng, Z.L., Wu, X.J., Zhang, W.T., Qin, H.B., 2018. Effect of organic type and moisture on CO2/CH4 competitive adsorption in kerogen with implications for CO2 sequestration and enhanced CH4 recovery. Appl. Energy 210, 28–43. https://doi.org/10.1016/j.apenergy.2017.10.122.
Huang, L., Ning, Z.F., Wang, Q., Qi, R.R., Cheng, Z.L., Wu, X.J., Zhang, W.T., Qin, H.B., 2019. Kerogen deformation upon CO2/CH4 competitive sorption: implications for CO2 sequestration and enhanced CH4 recovery. J. Petrol. Sci. Eng. 183, 106460 https://doi.org/10.1016/j.petrol.2019.106460.
Jackson, M.D., Alroudhan, A., Vinogradov, J., 2016. Zeta potential of intact natural limestone: impact of potential-determining ions Ca, Mg and SO4. Colloids Surf., A 493, 83–98. https://doi.org/10.1016/j.colsurfa.2015.11.068.
Jagadisan, A., Heidari, Z., 2021. Molecular dynamic simulation of the impact of thermal maturity and reservoir temperature on the contact angle and wettability of kerogen. Fuel 309, 122039. https://doi.org/10.1016/j.fuel.2021.122039.
Jin, Z., Firoozabadi, A., 2014. Effect of water on methane and carbon dioxide sorption in clay minerals by Monte Carlo simulations. Fluid Phase Equil. 382, 10–20. https://doi.org/10.1016/j.fluid.2014.07.035.
Jones, J.E., 1924. On the determination of molecular fields. II. From the equation of state of gas. Proc. Roy. Soc. A. 106, 463–477. https://doi.org/10.2307/94265.
Kasha, A., Al-Hashim, H., Abdallah, W., Taherian, R., Sauerer, B., 2015. Effect of Ca2+, Mg2+ and SO42 ions on the zeta potential of calcite and dolomite particles aged with stearic acid. Colloids Surf., A 482, 290–299. https://doi.org/10.1016/j.colsurfa.2015.05.043.
Lan, Q., Xu, M., Binazadeh, M., Dehghanpour, H., Wood, J.M., 2015. A comparative investigation of shale wettability: the significance of pore connectivity. J. Nat. Gas Sci. Eng. 27, 1174–1188. https://doi.org/10.1016/j.jngse.2015.09.064.
Le, N.P., Walsh, T.R., 2021. Force fields for water-surface interaction: is reproduction of the experimental water contact angle enough? Chem. Commun. 27, 3355–3358. https://doi.org/10.1039/D1CC00426C.
Li, Y.J., Chen, X., 2011. Fundamentals of Molecular Simulation. Central China Normal University Press, Hubei.
Li, J., Wang, F., 2017. Water graphene contact surface investigated by pairwise potentials from force-matching PAW-PBE with dispersion correction. J. Chem. Phys. 146, 054702 https://doi.org/10.1063/1.4974921.
Li, H., Xiao, C.Z., 2012. Wetting and interfacial properties of water nanodroplets in contact with graphene and monolayer boron-nitride sheets. ACS Nano 6, 2401–2409. https://doi.org/10.1021/nn204661d.
Li, A., Zhang, C., Zhang, Y.F., 2017. Thermal conductivity of graphene-polymer composites: mechanisms, properties, and applications. Polymers 9, 437. https://doi.org/10.3390/polym9090437.
Li, X., Kang, Y., Zhou, L., 2018. Investigation of gas displacement efficiency and storage capability for enhanced CH4 recovery and CO2 sequestration. J. Petral. Sci. Eng. 169, 485–493. https://doi.org/10.1016/j.petrol.2018.06.006.
Li, P., Zhang, J.C., Rezaee, R., Dang, W., Li, X.K., Fauziah, C.A., Nie, H.K., Tang, X., 2021. Effects of swelling-clay and surface roughness on the wettability of transitional shale. J. Pet. Sci. Eng. 196, 108007 https://doi.org/10.1016/j.petrol.2020.108007.
Lin, K., Yuan, Q., Zhao, Y.P., 2017. Using graphene to simplify the adsorption of methane on shale in MD simulations. Comput. Mater. Sci. 133, 99–107. https://doi.org/10.1016/j.commatsci.2017.03.010.
Lin, Q.D., Li, S.H., Feng, C., Wang, X.Q., 2021. Cohesive fracture model of rocks based on multi-scale model and Lennard-Jones potential. Eng. Fract. Mech. 246, 107627 https://doi.org/10.1016/j.engfracmech.2021.107627.
Liu, J., Xie, L.Z., He, B., Gan, Q., Zhao, P., 2021. Influence of anisotropic and heterogeneous permeability coupled with in-situ stress on CO2 sequestration with simultaneous enhanced gas recovery in shale: quantitative modeling and case study. Int. J. Greenh. Gas Control 104, 103208. https://doi.org/10.1016/j.ijggc.2020.103208.
Lou, Z.S., Chen, Q.W., 2013. Synthesis of Diamond and Carbon Materials by Chemical Reduction of Carbon Dioxide. Beijing University of Posts and Telecommunications Press, Beijing.
Loucks, R.G., Reed, R.M., Ruppel, S.C., Hammes, U., 2012. Spectrum of pore types and networks in mudrocks and a descriptive classification for matrix-related mudrock pores. AAPG Bull. 96, 1071–1098. https://doi.org/10.1306/08171111061.
Louk, K., Ripepi, N., Luxbacher, K., Gilliland, E., Tang, X., Keles, C., Schlosser, C., Diminick, E., Keim, S., Amante, J., Mischael, K., 2017. Monitoring CO2 storage and enhanced gas recovery in unconventional shale reservoirs: results from the Morgan County, Tennessee injection test. J. Nat. Gas Sci. Eng. 45, 11–25. https://doi.org/10.1016/j.jngse.2017.03.025.
Lu, H., Sha, S.M., Yang, S.L., Wu, J.D., Ma, J.F., Hou, C.P., Sheng, Z.L., 2021. The coating and reduction of graphene oxide on meshes with inverse wettability for continuous water/oil separation. Appl. Surf. Sci. 538, 147948 https://doi.org/10.1016/j.apsusc.2020.147948.
Ma, Y., Lu, G.W., Shao, C.J., Li, X., 2019. Molecular dynamics simulation of hydrocarbon molecule adsorption on kaolinite (0 0 1) surface. Fuel 237, 989–1002. https://doi.org/10.1016/j.fuel.2018.10.063.
Ma, B.Y., Hu, Q.H., Yang, S.Y., Qiao, H.G., Pu, X.G., Han, W.Z., 2022. An improved liquid-liquid extraction technique to determine shale wettability. Mar. Petrol. Geol. 138, 105538 https://doi.org/10.1016/j.marpetgeo.2022.105538.
Morrow, N.R., 1990. Wettability and its effect on oil recovery. J. Petrol. Technol. 42, 1476–1484. https://doi.org/10.2118/21621-PA.
Muhammad, A., Nilesh, K.J., Nilanjan, P., Alireza, K., Hussein, H., Mohammad, S., 2021. Recent advances in carbon dioxide geological storage, experimental procedures, influencing parameters, and future outlook. Earth Sci. Rev. 225, 103895 https://doi.org/10.1016/j.earscirev.2021.103895.
Muhammad, A., Pan, B., Yekeen, N., Al-Anssari, S., Keshavarz, A., Iglauer, S., Hoteit, H., 2022. Assessment of wettability and rock-fluid interfacial tension of caprock: implications for hydrogen and carbon dioxide geo-storage. Int. J. Hydrogne. Energ. 47, 14104–14120. https://doi.org/10.1016/j.ijhydene.2022.02.149.

Pan, B., Li, Y., Wang, H., Jones, F., Lglauer, S., 2018. CO2 and CH4 wettabilities of organic-rich shale. Energy Fuel. 32, 1914–1922. https://doi.org/10.1021/acs.energyfuels. 7b01147.
Pan, B., Jone, F., Huang, Z.Q., Yang, Y.F., Li, Y.J., Hejazii, S.H., Iglauer, S., 2019. Methane (CH4) wettability of clay-coated quartz at reservoir conditions. Energy Fuels 32, 788–795. https://doi.org/10.1021/acs.energyfuels.8b03536.
Pan, B., Yin, X., Iglauer, S., 2020a. A review on clay wettability: from experimental investigations to molecular dynamics simulations. Adv. Colloid. Interfac. 285, 102266 https://doi.org/10.1016/j.cis.2020.102266.
Pan, B., Li, Y.j., Zhang, M.S., Wang, X.P., Iglauer, S., 2020b. Effect of total organic carbon (TOC) content on shale wettability at high pressure and high temperature conditions. J. Pet. Sci. Eng. 193, 107374 https://doi.org/10.1016/j.petrol.2020.107374.
Paylor, Adrian, 2017. The social-economic impact of shale gas extraction: a global perspective. Third World Q. 38, 1–16. https://doi.org/10.1080/01436597.2016.1153420.
Pham, A.V., Fang, T.H., Nguyen, V.T., Chen, T.H., 2021. Impact and wetting properties of Au nanoparticle on Cu (001) textured surfaces by molecular dynamics. Mater. Chem. Phys. 272, 125039 https://doi.org/10.1016/j.matchemphys.2021.125039.
Price, E.K., Bansala, T., Achee, T.C., Sun, W., Green, M.J., 2019. Tunable dispersibility and wettability of graphene oxide through one-pot functionalization and reduction. J. Colloid Interface Sci. 552, 771–780. https://doi.org/10.1016/j.jcis.2019.05.097.
Qin, C., Jiang, Y.D., Zhou, J.P., Zuo, S.Y., Chen, S.W., Liu, Z.J., Yin, H., Li, Y., 2022. Influence of supercritical CO2 exposure on water wettability of shale: implications for CO2 sequestration and shale gas recovery. Energy 242, 122551. https://doi.org/10.1016/j.energy.2021.122551.
Rego, F.B., Eltahan, E., Sepehrnoori, K., 2022. Wettability alteration and improved oil recovery in unconventional resources. J. Petrol. Sci. Eng. 212, 110292 https://doi.org/10.1016/j.petrol.2022.110292.
Salehi, M., Johnson, S.J., Liang, J.T., 2008. Mechanistic study of wettability alteration using surfactants with applications in naturally fractured reservoirs. Langmuir 24, 14099. https://doi.org/10.1021/la802464u.
Savin, A.V., Mazo, M.A., 2020. The COMPASS force field: validation for carbon nanoribbons. Physica. E. 118, 113937 https://doi.org/10.1016/j.physe.2019.113937.
Sayyouh, M.H., Dahab, A.S., Omar, A.E., 1990. Effect of clay content on wettability of sandstone reservoirs. J. Petrol. Sci. Eng. 4, 119–125. https://doi.org/10.1016/0920-4105(90)90020-4.
Sharifigaliuk, H., Mahmood, S.M., Ahmad, M., Khosravi, V., Matýsek, D., 2022. Comparative analysis of conventional methods for the evaluation of wettability in shales. J. Pet. Sci. Eng. 208, 109729 https://doi.org/10.1016/j.petrol.2021.109729.
Siddiqui, M.A.Q., Ali, S., Fei, H., Roshan, H., 2018. Current understanding of shale wettability: a review on contact angle measurements. Earth Sci. Rev. 181, 1–11. https://doi.org/10.1016/j.earscirev.2018.04.002.
Singh, K., Anabaraonye, B.U., Blunt, M.J., Crawshaw, J., 2018. Partial dissolution of carbonate rock grains during reactive CO2-saturated brine injection under reservoir conditions. Adv. Water Resour. 122, 27–36. https://doi.org/10.1016/j.advwatres.2018.09.005.
Sohrab, Z., Nima, R., Ali, L., 2018. Applications of hybrid models in chemical, petroleum, and energy systems: a systematic review. Appl. Energy 228, 2539–2566. https://doi.org/10.1016/j.apenergy.2018.06.051.
Stevar, M., Bhm, C., Notarki, K.T., Trusler, J.P.M., 2019. Wettability of calcite under carbon storage conditions. Int. J. Greenh. Gas Control 84, 180–189. https://doi.org/10.1016/j.ijggc.2019.03.024.
Sun, H., 1998. COMPASS: an ab initio force-field optimized for condensed-phase applications—overview with details on alkane and benzene compounds. J. Phys. Chem. B 102, 7338–7364. https://doi.org/10.1021/jp980939v.
Tang, X.H., Zhu, H., Wang, H.B., Li, F.X., Zhou, T., He, J.Y., 2022. Geomechanics evolution integrated with hydraulic fractures, heterogeneity and anisotropy during shale gas depletion. Geomech. Energy. Envir. 100321 https://doi.org/10.1016/j.gete.2022.100321.
Tayari, F., Blumsack, S., Dilmore, R., Mohaghegh, S.D., 2015. Techno-economic assessment of industrial CO2 storage in depleted shale gas reservoirs. J. Unconv. Oil. Gas. Res. 11, 82–94. https://doi.org/10.1016/j.juogr.2015.05.001.
Tenney, C.M., 2009. Molecular Simulation of Carbon Dioxide Adsorption for Carbon Capture and Storage. University of Michigan.
Tetteh, J., Bai, S., Kubelka, J., Piri, M., 2021. Surfactant-induced wettability reversal on oil-wet calcite surfaces: experimentation and molecular dynamics simulations with scaled-charges. J. Colloid Interface Sci. 609, 890–900. https://doi.org/10.1016/j.jcis.2021.11.080.
Tirjoo, A., Bayati, B., Rezaei, H., Rahmati, M., 2019. Molecular dynamics simulations of asphaltene aggregation under different conditions. J. Pet. Sci. Eng. 177, 392–402. https://doi.org/10.1016/j.petrol.2019.02.041.
Valluri, M.K., Alvarez, J.O., Schechter, D.S., 2016. Study of the rock/fluid interactions of sodium and calcium brines with ultra-tight rock surfaces and their impact on improving oil recovery by spontaneous imbibition. SPE. Low. Perm. Symposium. https://doi.org/10.2118/180274-ms.
Wang, X.P., Mou, C.L., Ge, X.Y., Chen, X.W., Zhou, K.K., Wang, Q.Y., Liang, W., 2015. Mineral composition characteristics and evaluation of black rock series of Longmaxi formation in southern Sichuan and its adjacent areas. Acta Petrol. Sin. 36, 150–162. https://doi.org/10.7623/syxb201502003.
Xia, D., Li, Q., Xue, Q.Z., Liang, C.Y., Dong, M.D., 2016. Super flexibility and stability of graphene nanoribbons under severe twist. Phys. Chem. Chem. Phys. 18, 18406–18413. https://doi.org/10.1039/c6cp02580c.
Xin, G., Yao, T., Sun, H., Scott, S.M., Shao, D., Wang, G., Lian, J., 2015. Highly thermally conductive and mechanically strong graphene fibers. Science 349, 1083–1087. https://doi.org/10.1126/science.aaa6502.
Xu, L., Myers, M., Li, Q., White, C., Zhang, X.Y., 2020. Migration and storage characteristics of supercritical CO2 in anisotropic sandstones with clay interlayers based on X-CT experiments. J. Hydrol. 580, 124239 https://doi.org/10.1016/j.jhydrol.2019.124239.
Xu, Y.Y., Liu, X.G., Hu, Z.M., Shao, N., Duan, X.G., Chang, J., 2022. Production effect evaluation of shale gas fractured horizontal well under variable production and variable pressure. J. Nat. Gas Sci. Eng. 97, 104344 https://doi.org/10.1016/j.jngse.2021.104344.
Xue, Q.Z., Tao, Y.H., Liu, Z.L., Lu, S.F., Li, X.F., Wu, T.T., Jin, Y.K., 2015. Mechanism of oil molecules transportation in nano-sized shale channel: MD simulation. RSC Adv. 5, 25684–25692. https://doi.org/10.1039/C4RA16682E.
Yassin, M.R., Begum, M., Dehghanpour, H., 2017. Organic shale wettability and its relationship to other petrophysical properties: a Duvernay case study. Int. J. Coal Geol. 169, 74–91. https://doi.org/10.1016/j.coal.2016.11.015.
Yoshimitsu, Z., Nakajima, A., Watanable, T., Hashimoto, K., 2002. Effects of surface structure on the hydrophobicity and sliding behavior of water droplets. Langmuir 18, 5818–5822. https://doi.org/10.1021/la020088p.
Yu, D.Y., 2014. Comprehensive Experiment of Food Engineering. China Forestry Press, Beijing.
Yu, X.R., Li, J., Chen, Z.X., Wu, K.L., Zhang, L.Y., Hui, G., Yang, M., 2020. Molecular dynamics computations of brine-CO2/CH4-shale contact angles: implications for CO2 sequestration and enhanced gas recovery. Fuel 280, 118590. https://doi.org/10.1016/j.fuel.2020.118590.
Yu, T., Qi, L., Hu, B., Tan, Y.S., Xu, L., 2021. Molecular dynamics simulation of the interfacial wetting behavior of brine/sandstone with different salinities. Colloids Surf., A 632, 127807. https://doi.org/10.1016/j.colsurfa.2021.127807.
Yuan, J.H., Luo, D.K., Feng, L.Y., 2015. A review of the technical and economic evaluation techniques for shale gas development. Appl. Energy 148, 49–65. https://doi.org/10.1016/j.apenergy.2015.03.040.
Yuan, Q., Zhu, X., Lin, K., Zhao, Y.B., 2015. Molecular dynamics simulations of the enhanced recovery of confined methane with carbon dioxide. Phys. Chem. Chem. Phys. 17, 31887 https://doi.org/10.1039/c5cp06649b.
Zhao, X., Jin, H., 2020. Correlation for self-diffusion coefficients of H2, CH4, CO, O2 and CO2 in supercritical water from molecular dynamics simulation. Appl. Therm. Eng. 171, 114941 https://doi.org/10.1016/j.applthermaleng.2020.114941.
Zhong, J., Wang, P., Zhang, Y., Yan, Y.G., Hu, S.Q., Zhang, J., 2013. Adsorption mechanism of oil components on water-wet mineral surface: a molecular dynamics simulation study. Energy 59, 295–300. https://doi.org/10.1016/j.energy.2013.07.016.
Zhou, J.P., Tian, S.F., Zhou, L., Xian, X.F., Yang, K., Jiang, Y.D., Zhang, C.P., Guo, Y.W., 2020. Experimental investigation on the influence of sub-and super-critical CO2 saturation time on the permeability of fractured shale. Energy 191, 116574. https://doi.org/10.1016/j.energy.2019.116574.
Zhou, J., Zhang, J., Yang, J., Jin, Z.H., Luo, K.H., 2021. Mechanisms for kerogen wettability transition from water-wet to CO2-wet: implications for CO2 sequestration. Chem. Eng. J. 428, 132020 https://doi.org/10.1016/j.cej.2021.132020.
Zhu, L., Xue, Q.Z., Li, X.F., Jin, Y.K., Zheng, H.X., Wu, T.T., 2015. Theoretical prediction of hydrogen separation performance of two-dimensional carbon network of fused pentagon. ACS Appl. Mater. Interfaces 7, 28502–28507. https://doi.org/10.1021/acsami.5b09648.